12970–12985 *Nucleic Acids Research, 2021, Vol. 49, No. 22* *Published online 8 December 2021*
https://doi.org/10.1093/nar/gkab1198

Perinuclear positioning of endosomes can affect PS-ASO activities

Xue-hai Liang [1,*], Joshua G Nichols[1], Dario Tejera[2] and Stanley T. Crooke [1]

[1]Core Antisense Research, Ionis Pharmaceuticals, Inc., Carlsbad, CA 92010, USA and [2]Neurology, Ionis Pharmaceuticals, Inc., Carlsbad, CA 92010, USA

Received August 24, 2021; Revised November 16, 2021; Editorial Decision November 17, 2021; Accepted November 22, 2021

ABSTRACT

Phosphorothioate (PS) modified antisense oligonucleotide (ASO) drugs that act on cellular RNAs must enter cells and be released from endocytic organelles to elicit antisense activity. It has been shown that PS-ASOs are mainly released by late endosomes. However, it is unclear how endosome movement in cells contributes to PS-ASO activity. Here, we show that PS-ASOs in early endosomes display Brownian type motion and migrate only short distances, whereas PS-ASOs in late endosomes (LEs) move linearly along microtubules with substantial distances. In cells with normal microtubules and LE movement, PS-ASO-loaded LEs tend to congregate perinuclearly. Disruption of perinuclear positioning of LEs by reduction of dynein 1 decreased PS-ASO activity, without affecting PS-ASO cellular uptake. Similarly, disruption of perinuclear positioning of PS-ASO-LE foci by reduction of ER tethering proteins RNF26, SQSTM1 and UBE2J1, or by overexpression of P50 all decreased PS-ASO activity. However, enhancing perinuclear positioning through reduction of USP15 or over-expression of RNF26 modestly increased PS-ASO activity, indicating that LE perinuclear positioning is required for ensuring efficient PS-ASO release. Together, these observations suggest that LE movement along microtubules and perinuclear positioning affect PS-ASO productive release.

INTRODUCTION

PS-ASOs must enter cells and reach the target RNAs in the cytosol and the nucleus to elicit antisense activity (1,2). It has been shown that PS-ASOs enter cells primarily via the endocytic pathways (1,3,4). Internalized PS-ASOs bud off from plasma membrane and transport quickly into early endosomes (EEs) and late endosomes (LE), and finally localize to lysosomes. However, PS-ASO release from endocytic organelles is a relatively slow process and a rate limiting step affecting PS-ASO activity (1,5). Only a small portion of internalized PS-ASOs are released from the membraned endocytic organelles (6). LEs, or multivesicular bodies (MVBs) appear to be the major sites for productive PS-ASO release (1,3,7–9).

Recently we identified the pathways and protein factors involved in PS-ASO intracellular transport and endosomal release (10). We found that many pathways and proteins are involved and can act in parallel to affect PS-ASO endosomal release (1). For example, upon PS-ASO cellular uptake, endoplasmic reticulum (ER)-derived COPII vesicles and trans-Golgi network (TGN)-derived M6PR vesicles are recruited to LEs, mediated by Syntaxin 5 (STX5) and GRIP and Coiled-Coil Domain Containing 2 (GCC2) proteins, respectively, to independently facilitate PS-ASO release from LEs (5,11). These proteins and vesicles can relocalize to LEs upon PS-ASO cellular uptake, in a time- and dose-dependent manner, and the protein relocalization is most likely mediated by PS-ASO-protein interactions. Some additional proteins, such as Annexin A2 (ANXA2) and Golgi-58K, can also relocate to LEs after PS-ASO uptake and mediate endosomal release of PS-ASOs through different mechanisms, with ANXA2 affecting EE-to-LE maturation and endosomal release and Golgi-58K affecting the GCC2-M6PR transport pathway (12,13). These various proteins/vesicles may trigger PS-ASO release either through vesicular escape, or through membrane deformation when contacting LE limiting membranes. Additionally, PS-ASOs can also localize in intralumenal vesicles (ILVs) inside LE limiting membranes, and may be released through a back-fusion-mediated process (7,9,11,13). Due to the existence of multiple PS-ASO release pathways, blocking a particular pathway normally causes only modest defects in PS-ASO release and thus activity.

The above observations highlight the importance of LEs and TGN in productive PS-ASO release. However, since LEs (and other cellular organelles including Golgi and ER) undergo dynamic movement in cells, and can encounter other organelles during the movement (14), it is possible that LE movement might affect PS-ASO positioning and productive release, and subsequently antisense activity. However, such a possibility has not been thoroughly eval-

*To whom correspondence should be addressed. Tel: +1 760 603 3816; Fax: +1 760 603 2600; Email: Lliang@ionisph.com

uated for PS-ASOs. Microtubules are organized by the interaction of the minus end of the microtubules to the microtubule organizing center (MTOC) residing in the perinuclear region and the plus end of microtubules grows toward the plasma membrane (15). The perinuclear area appears to have important roles, since some organelles, including endosomes/lysosomes and Golgi, tend to localize to this region, and perinuclear translocation of certain proteins or enzymes was found to be important for their function (16).

Previous studies have demonstrated that LEs undergo bidirectional movements along microtubules (17). The migration toward the minus end of microtubules that are anchored to the MTOC is defined as retrograde transport (17–19). LE movement along microtubules depends on different motor proteins, with cytoplasmic Dynein 1 mainly responsible for movement towards minus end, and a set of kinesin proteins for the movement towards the plus end of microtubules (18). During the movement, LEs can encounter other cellular structures such as other microtubule structures, or other organelles including Golgi and ER, affecting the status of LEs (20). Indeed, ER-LE contact sites have been shown to affect LE maturation, positioning, and endosome fission (21). Recently, it was found that Ring Finger Protein 26 (RNF26), an ER-localized E3 ubiquitin-protein ligase, is required for tethering LEs to ER and for their perinuclear positioning; whereas Ubiquitin Specific Peptidase 15 (USP15) opposes RNF26 effect by allowing LE release from ER to move away from the perinuclear areas (22). The dynamic movement of LEs and their interactions with other organelles suggest a possibility that these events may affect PS-ASO release from LEs and subsequently antisense activity.

Here, we characterized the movement of PS-ASO containing endosomes, and found that PS-ASO containing EEs move within a short distance and in a largely non-linear fashion. EE movement and PS-ASO activity do not appear to depend on actin filaments in human cells. In contrast, we demonstrated that PS-ASO-containing LEs move along microtubules relatively rapidly over longer distances in the periphery of the cytoplasm, but the movement is slower and over a shorter distance in the perinuclear area. The movement of PS-ASO laden LEs can be affected by other cellular structures, including ER, altering the direction or pausing the movement. Importantly, disruption of microtubules using small molecules caused LE clumping and abolished perinuclear positioning. Disruption of perinuclear accumulation of LEs by siRNAs reducing dynein 1 or RNF26 and its partner proteins, or by over expression of P50 protein, all reduced PS-ASO activity. However, enhancing perinuclear accumulation of LEs by reduction of USP15 or over-expression of RNF26 increased PS-ASO activity. Altogether, our results strongly suggest that perinuclear positioning of LEs can enhance PS-ASO activity, most likely by enhancing PS-ASO release from LEs.

MATERIALS AND METHODS

Reagents and materials

Colchicine (C9754), demecolcine (D7385), nocodazole (SML1665) and latrunculin (L5163) were purchased from Sigma. Transferrin-AF647 (T23366), CellLight^{TM} virus for GFP-Tubulin (C10613), GFP-Actin (C10506) and GFP-Late endosome (C10588) were purchased from ThermoFisher. The P50 expression plasmid (RC214771) and RNF26 over expression plasmid (RC200846) were from Origene.

siRNAs and primer probe sets (Supplementary Table S1), antibodies (Supplementary Table S2), and ASOs (Supplementary Table S3) are listed in Supplementary Information.

Cell culture, siRNA and PS-ASO treatment

HeLa, A431, GFP-Rab7 expressing SVGA cells (a kind gift from Dr Tomas Kirchhausen's lab), and mouse MHT cells were grown in Dulbecco's modified Eagle's medium (DMEM) supplemented with 10% fetal bovine serum (FBS), 0.1 μg/ml streptomycin, and 100 units/ml penicillin. Cells were seeded at 70% confluency one day before siRNA transfection or PS-ASO treatment. siRNAs were transfected at 3 nM final concentration into HeLa cells or at 10 nM final concentration for A431 and MHT cells using Lipofectamine RNAiMAX (Life Technologies), according to the manufacturer's protocol. At 48 h after siRNA transfection, cells were reseeded into 96-well plates for PS-ASO activity or uptake assays or were seeded into collagen-coated glass-bottom dishes (MatTek) at 70% confluency for immunofluorescent staining and imaging.

ASO activity assay

Cells grown in 96-well plates were added with PS-ASOs at different concentrations without transfection reagent (free uptake), and 18–24 h later, cells were collected for RNA preparation. For transfection, cells grown in 96-well plates were refed with pre-warmed Opti medium, and transfected with PS-ASOs at different concentrations using Lipofectamine 2000, as described previously (23). 4–6 h after transfection, cells were collected for RNA preparation. For small molecular inhibitor treatment, cells were treated with the inhibitors in complete DMEM medium first for different times as described in figure legends, then medium was changed with fresh medium and ASOs were then immediately added to the medium. Cells were collected after overnight PS-ASO incubation. Alternatively, cells were first incubated with PS-ASOs for different times, followed by treatment with various inhibitors for 2–4 h, as described in figure legends. Next, cells were collected for RNA preparation. PS-ASO activity was determined by qRT-PCR for the levels of PS-ASO-targeted RNAs.

RNA preparation and qRT-PCR

Total RNA was prepared using a RNeasy mini kit (Qiagen) from cells grown in 96-well plates based on the manufacturer's protocol. qRT-PCR was performed in triplicate using TaqMan primer probe sets as described previously (24). Briefly, approximately 50 ng total RNA in 5 μl water was mixed with 0.3 μl primer probe sets containing forward and reverse primers (10 μM of each) and fluorescently labeled probe (3 μM), 0.5 μl RT enzyme mix (Qiagen), 4.2 μl RNase-free water, and 10 μl of 2× PCR reaction buffer in a 20 μl reaction. Reverse transcription was performed at

48°C for 10 min, followed by 94°C for 10 min, and then 40 cycles of PCR were conducted at 94°C for 30 s, and 60°C for 30 s within each cycle using the StepOne Plus RT-PCR system (Applied Biosystems). The mRNA levels were normalized to the amount of total RNA present in each reaction as determined for duplicate RNA samples using the Ribogreen assay (Life Technologies). Statistical analyses were performed from three independent experiments using Prism with either t-test or F-test for curve comparison based on non-linear regression (dose-response curves) for XY analyses, using equation 'log (agonist) versus normalized response – variable slope'. The Y axis (relative level) was used as the normalized response.

PS-ASO uptake assay

A431 cells were seeded into 96-well plates, incubated overnight, and Cy3-labeled PS-ASO 446654 was added to the medium. After 3 h, cells were washed three times with 1 × PBS, trypsinized, and pelleted by centrifugation. Cell pellet was washed once with 1× PBS supplemented with 3% FBS, to remove residual medium and external PS-ASOs. Cells were then resuspended in 1× PBS supplemented with 3% FBS for analysis by flow cytometry using an Attune NxT Flow Cytometer (ThermoFisher Scientific).

Western analyses

Cell pellets were lysed by incubation at 4°C for 30 min in RIPA buffer (50 mM Tris–HCl, pH 7.4, 1% Triton X-100, 150 mM NaCl, 0.5% sodium deoxycholate, and 0.5 mM EDTA). Proteins were collected by centrifugation. Approximately 20–40 μg protein were separated on 6–12% NuPAGE Bis-Tris gradient SDS-PAGE gels (Life Technologies), and transferred onto PVDF membranes using the iBLOT transfer system (Life Technologies). The membranes were blocked with 5% non-fat dry milk in 1 × PBS at room temperature for 30 min. Membranes were then incubated with primary antibodies at room temperature for 2 h or at 4°C overnight. After three washes of 5 min each with wash buffer (0.05% Tween-20 1× PBS), the membranes were incubated with appropriate HRP-conjugated secondary antibodies (1:2000) at room temperature for 1 h. After three washes with wash buffer, images were developed using Immobilon Forte Western HRP Substrate (Millipore), and visualized using ChemiDoc system (Bio-Rad).

Immunofluorescence staining and confocal imaging

For immunofluorescence staining, cells were washed with 1× PBS, fixed with 4% paraformaldehyde for 0.5 h at room temperature, and permeabilized for 4 min with 0.1% Triton in 1× PBS. After blocking at room temperature for 30 min with 1 mg/ml BSA in 1 × PBS, cells were incubated with primary antibodies (1:100–1:300) in 1 mg/ml BSA in 1 × PBS for 2–4 h, washed three times (5 min each) with 0.1% nonyl phenoxypolyethoxylethanol-40 (NP-40) in 1× PBS, and incubated for 1 h with secondary antibody conjugated with fluorophores (1:200). After washing three times, cells were mounted with anti-fade reagent containing DAPI (Life Technologies). Images were acquired with 100× objective lens at 4 μs/pixel sampling speed, using confocal microscope (Olympus FV-1000) and processed using FV-10 ASW 3.0 Viewer software (Olympus). For staining within 2 h of PS-ASO addition, cells were washed three times with acidic buffer (0.1 M acetic acid, 500 mM NaCl) and one time with 1× PBS, to remove cell surface associated ASOs before fixation.

For live cell imaging, HeLa cells grown in glass-bottom dishes were first transduced for 24 h with virus expressing various GFP-labelled markers for Tubulin, actin, or LEs. Next, cells were incubated with 2 μM PS-ASO 446654 for different times, as indicated in figure legends, with or without treatment by different inhibitors. Medium was then changed to pre-warmed FluoroBrite DMEM Media (Life Technologies), and images were continuously recorded using 100X objective lens and 2 μs/pixel sampling speed in an environmental chamber at 37°C for 2–10 min. Movies and images were generated using FV-10 ASW 3.0 Viewer software. Time projection data were generated from 2-min movies, by overlaying all continuous images taken at ∼3 seconds interval.

Quantification and measurement of images

Measurement of the distances between ASO foci and nuclei was performed using Fiji-ImageJ (25). Briefly, the positions of the nucleus (X_n, Y_n) and ASO foci (X_i, Y_i) were measured in pixels, and the distances between each ASO focus and the nucleus were calculated using equation: distance = $((Xi– X_n)^2+(Y_i – Y_n)^2)^{0.5}$. The results obtained from ∼10 cells in each case were plotted using Excel. Measurement of the movement of ASO foci was performed using Imaris (Oxford Instruments). Briefly, time-lapse movies were reconstructed using the 'spots' function with an automatic background subtraction and an autoregressive motion algorithm for particle tracking. For each individual cell, the periphery and perinuclear area, as well as the whole cell were measured for the mean speed, and total PS-ASO trafficking distance every 1.25 s for ∼60 s. The mean speeds and total distances at each time point were plotted in excel based on the measurement from six cells, and P-values were calculated based on unpaired t-test using Prism.

RESULTS

PS-ASO containing endosomes showed different movements at different times and positions in cells after cellular uptake of PS-ASOs

To characterize PS-ASO movement after internalization, Cy3-labeled PS-ASOs were incubated with HeLa cells expressing GFP-Tubulin for 20 or 45 min, at which times PS-ASOs can localize to EEs and LEs, respectively, or at 2 and 6 h, at which times the majority of PS-ASOs localize to LEs and lysosomes (12). Live cell images were taken using confocal microscopy. As expected, 20 min after PS-ASO incubation, a few PS-ASO foci were detected in cells (Figure 1A), mainly localized at EEs as determined by co-localization with EE marker protein Rab5 (Supplementary Figure S1A). These PS-ASO-containing EEs showed largely non-linear movement with relatively short distance, as can be seen from the time projection image (Figure 1A,

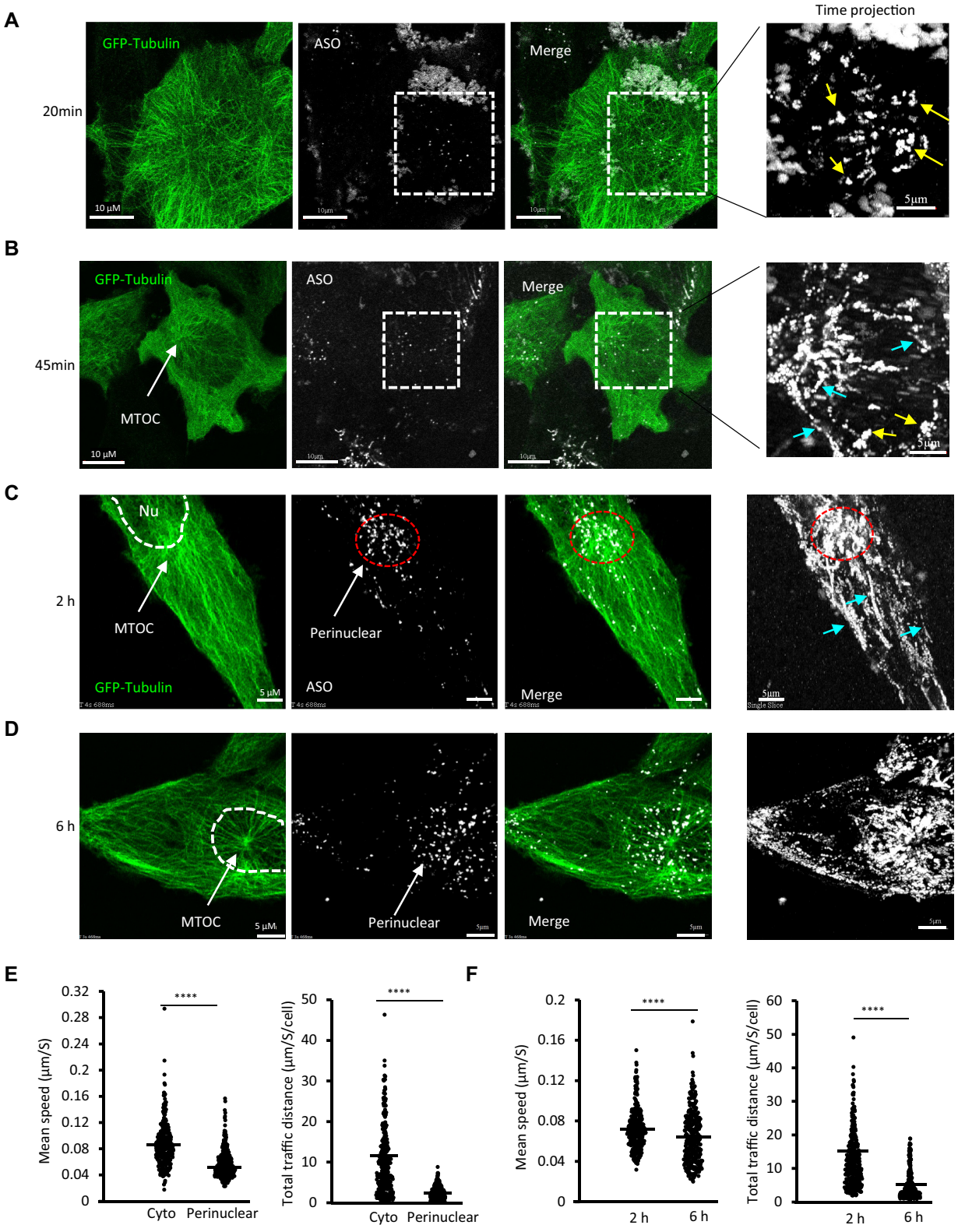

Figure 1. PS-ASO-containing endosomes tend to localize to perinuclear areas in a time dependent manner in live cells. Live cell imaging of PS-ASOs in HeLa cells expressing GFP-Tubulin at 20 min (**A**), 45 min (**B**), 2 h (**C**) and 6 h (**D**) after PS-ASO incubation. Images were recorded for ∼2 min, and time projections of PS-ASO foci are shown in right panels. MTOC, microtubule organizing center. Nu, nucleus. The perinuclear accumulation of PS-ASO foci is indicated with red circles. In right panels, Brownian movement is exemplified with yellow arrows, and linear movement with blue arrows. Scale bars are indicated in figures. (**E**) Quantification of the mean speed (left panel) and total trafficking distance (right panel) of PS-ASO foci in periphery cytoplasmic area (Cyto) or in perinuclear areas, as measured from six cells in movies taken at 2 h after PS-ASO incubation, as described in Materials and Methods. (**F**) Quantification of the mean speed (left panel) and total trafficking distance (right panel) of PS-ASO foci in whole cells (six cells each) from movies taken at 2 h or 6 h after PS-ASO incubation. P values were calculated based on unpaired t-test using Prism. ****$P < 0.0001$.

right panel) and live cell movies (Supplemental Mov-1). At 45 min, many PS-ASO-containing foci colocalized with Rab7 (Supplementary Figure S1B), a LE marker protein, suggesting that at this time, many ASO-containing EE already matured to LEs, consistent with our previous observations (12). At this time, some PS-ASO foci showed liner movement with longer distance (Cyan arrows), although some PS-ASO foci still showed non-linear movement with shorter range (yellow arrows) (Figure 1B, right panel, and Supplemental Mov-2).

At 2 h after PS-ASO incubation, most PS-ASO-foci co-stained with Rab7 (Supplementary Figure S1C), suggesting that most internalized PS-ASOs localized to LEs. At this time, PS-ASO foci showed dominantly linear movement over longer distances, especially in the periphery of the cytoplasm of the cells (Figure 1C, Supplemental Mov-3), suggesting a rapid, linear movement of LEs. However, at the perinuclear area where more PS-ASO foci localized than at the periphery, PS-ASO foci showed mostly non-linear movement over shorter distances, indicating that around the MTOC, the PS-ASO containing LEs have slower and more localized movement compared with that in the peripheral cytoplasmic areas. Similarly, at 6 h after PS-ASO incubation, PS-ASO foci tended to localize to the perinuclear area, where PS-ASO foci also showed slower movement over shorter distance than at the peripheral areas (Figure 1D, Supplemental Mov-4). This is further supported by the quantification results of the mean trafficking speed and total trafficking distance of PS-ASO foci in the periphery and perinuclear areas (Figure 1E). In addition, slower speed and shorter trafficking distance of total cellular PS-ASO foci were observed at 6 h relative to that at 2 h after PS-ASO incubation (Figure 1F), consistent with the observations that at 6h, majority of PS-ASO foci already accumulated at perinuclear areas.

Together, these results indicate that upon internalization, PS-ASOs in EEs showed mostly non-linear movement over shorter distances; whereas when PS-ASOs were localized to LEs, PS-ASOs moved over longer distances in a linear manner in the periphery of the cytoplasm. Overtime, PS-ASO containing LEs exhibited a net migration toward the cytoplasmic perinuclear area and once there they were engaged in non-linear, more localized movements. These observations are consistent with previous findings that LEs can have both rapid, linear movement in peripheral cytoplasmic regions and slower, non-linear movements in the perinuclear areas (17).

The actin network has minor effects on ASO-EE movement and PS-ASO activity

Although actin is required for clathrin-dependent endocytosis in yeast by facilitating membrane invagination and vesicle budding from the plasma membrane, in mammalian cells actin only affects a subset of clathrin-mediated uptake (18). In yeast, endosomes can move along actin cables, however, endosomal movement is largely microtubule dependent in human cells (26,27). To examine whether PS-ASO-containing EEs can move along actin filaments, HeLa cells expressing GFP-actin were incubated with Cy3-PS-ASOs for 15 min to allow PS-ASOs enter EEs, and PS-ASO movement was recorded in live cells. No obvious colocalization between PS-ASOs and actin filaments was found (Figure 2A). PS-ASOs, mostly in EEs at this time, showed predominately Brownian movement and did not obviously move along the actin filaments (Supplemental Mov-5). However, certain PS-ASO-containing endosomes can move across actin filaments (Figure 2B, Supplemental Mov-6). These results suggest that the movement of PS-ASO containing EE does not substantially depend on actin filaments.

To determine if actin filaments are involved in PS-ASO uptake and activity, A431 cells were treated for different times with latrunculin A to disrupt the actin network, followed by incubation for 16 h with RNase H1-dependent gapmer PS-ASOs targeting *NCL* and *drosha* mRNAs or nuclear Malat1 RNA. A431 cells were used since these cells show robust antisense activity when PS-ASOs are delivered by free uptake. The activity of PS-ASOs was evaluated by qRT-PCR quantification for the levels of the target RNAs. The results showed that pretreatment with latrunculin for 2–6 h did not substantially affect the antisense activity of PS-ASOs (Figure 2C), although under these conditions the actin network was disrupted (Supplementary Figure S2). These results suggest that actin filaments may not be important for PS-ASO cellular uptake and endosomal release. To further confirm this possibility, cells were first incubated with PS-ASOs to allow normal uptake and endosomal transport, followed by treatment with latrunculin for different times. Again, such treatment did not substantially affect the activity of PS-ASOs (Figure 2D). Together, these results indicate that the actin network is not essential for PS-ASO cellular uptake and endosomal release in these cells.

PS-ASO-containing LEs move along microtubules that contribute to the perinuclear localization

To determine if perinuclear concentration of PS-ASO containing LEs is a result of traffic along the microtubule network, HeLa cells incubated with Cy3-PS-ASOs for 6 h were stained for Beta-tubulin (TUBB) and Rab7. Most PS-ASOs colocalized with the LE marker protein Rab7, and nearly all PS-ASO foci appeared to be associated with microtubule structures (Figure 3A). Next, Cy3-PS-ASOs were incubated for 6 h with HeLa cells expressing GFP-Tubulin, and PS-ASO movement was recorded in live cells. The results showed that PS-ASO containing LEs indeed can move along the microtubule structures, as indicated for a particular LE in snapshots (Figure 3B), and in a live cell movie (Supplemental Mov-7). The movement of some PS-ASO containing LEs can be affected when encountering other microtubule structures, leading to an altered direction or slower movement, consistent with previous observations that LEs can move in a 'stop and go' fashion (20).

LEs can move relatively rapidly along microtubules at the periphery of the cytoplasm towards either the minus end (MTOC in the perinuclear area) or toward the plus end at the cell periphery (28). In the perinuclear area, the LE movement is slower with short distance (Figure 1). These observations suggest that PS-ASO containing LEs around the MTOC area have limited movement. Indeed, the perinuclear PS-ASO colocalizes with the MTOC, resulting in

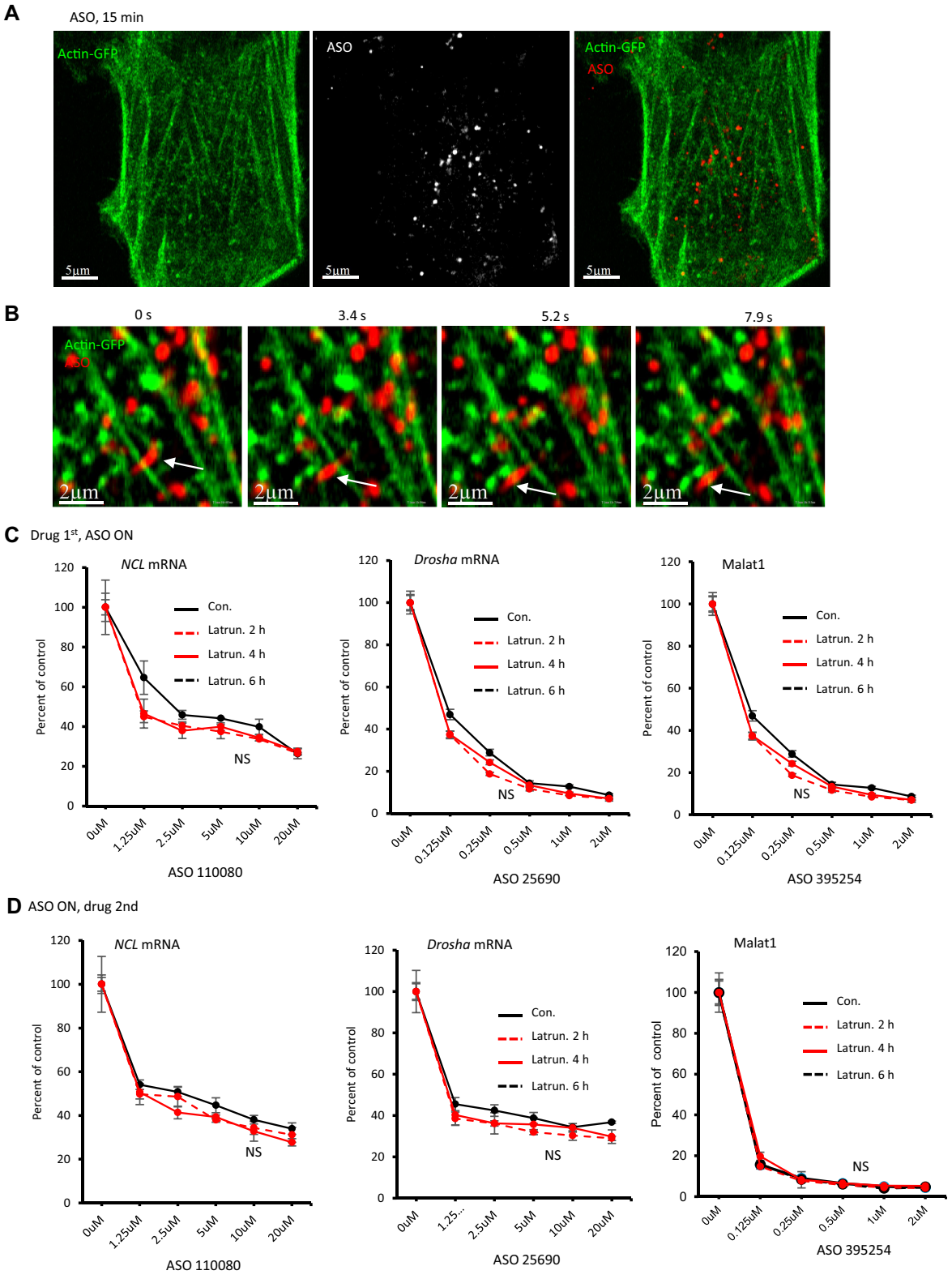

Figure 2. Actin networks do not play important roles in PS-ASO activity. (**A**) live cell imaging of HeLa cells expressing GFP-actin incubated with PS-ASOs for 15 min. (**B**) live cell imaging of GFP-actin expressing Hela cells incubated with PS-ASOs for 20 min. Snapshots were taken at different times. The movement of a PS-ASO structure across an actin filament is marked with arrows. (**C**) qRT-PCR quantification of the levels of *NCL*, *drosha*, and malat1 RNAs in A431 cells. Cells were pretreated with latrunculin at 0.2 μg/ml for different times, then medium was replaced with fresh medium and PS-ASOs were added immediately. Cells were incubated overnight and RNA was prepared. (**D**) qRT-PCR quantification of the levels of *NCL*, *drosha* and Malat1 RNAs in A431 cells. Cells were incubated with PS-ASOs overnight, followed by treatment with latrunculin at 0.2 μg/ml for different times. Cells were then collected, and RNA prepared. Error bars are standard deviations from three independent experiments. P values were calculated based on F-test.

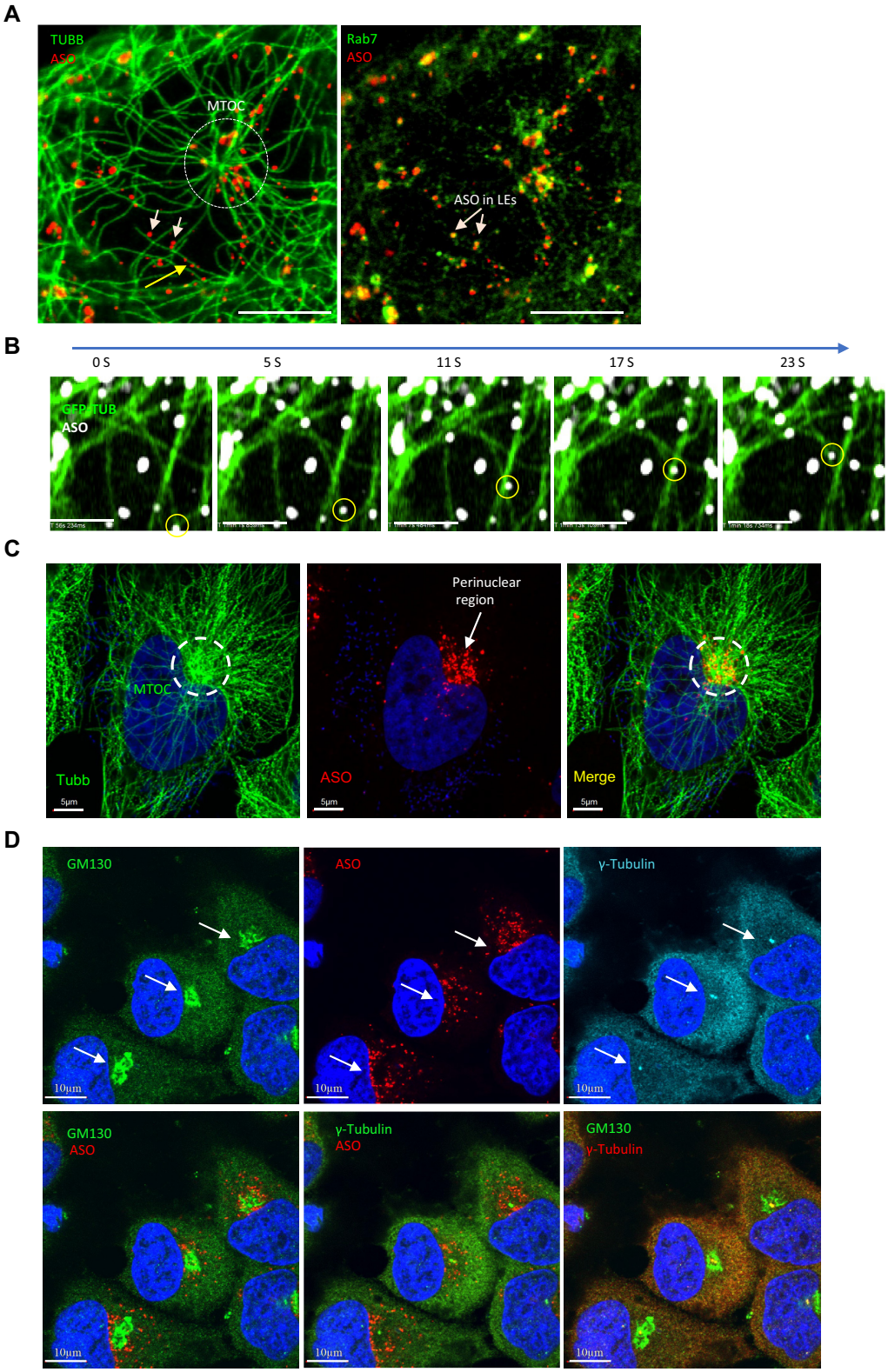

Figure 3. PS-ASO containing LEs move along microtubule networks. (**A**) Immunofluorescence staining of beta-tubulin (TUBB) and Rab7 in HeLa cells incubated for 6 h with 2 μM Cy3-labeled PS-ASO 446654. MTOC is marked with a dashed circle. PS-ASO-containing LEs associated with microtubules are exemplified with arrows. Scale bars, 5 μm. (**B**) Live cell imaging of PS-ASO foci in GFP-Tubulin expressing Hela cells incubated with PS-ASOs for 6 min. Snapshots were taken at different times. The movement of a PS-ASO structure along a microtubule is circled. Scale bars, 2 μm. (**C**) Immunofluorescence staining of TUBB and Rab7 in HeLa cells incubated for 8 h with 2 μM Cy3-labeled PS-ASO 446654. MTOC is circled and perinuclear accumulation of PS-ASO-LEs is indicated with an arrow. Scale bars, 5 μm. D) Immunofluorescence staining of GM130 and γ-Tubulin in HeLa cells incubated for 8 h with 2 μM Cy3-labeled PS-ASO 446654. MTOC regions are marked with arrows. Scale bars, 10 μm.

a cloud of PS-ASOs (Figure 3C). The localization of PS-ASOs at the MTOC is also supported by the observations that perinuclear PS-ASOs are adjacent to γ-tubulin, a protein localized to MTOC (29), and also adjacent to Golgi (Figure 3D), an organelle that is normally present at MTOC (30). However, ER and mitochondria do not exhibit obvious perinuclear positioning, as determined by co-staining with Calnexin and P32, markers of these two organelles, respectively (Supplementary Figure S3).

Disruption of the microtubule network altered PS-ASO-LE positioning

To further confirm that perinuclear enrichment of PS-ASO containing LEs is due to LE movement along microtubules, HeLa cells expressing GFP-tubulin was incubated with PS-ASOs for 6 h, then treated overnight with or without colchicine, a small molecule that disrupts microtubule network (31). In control cells, PS-ASOs appeared as some scattered LE foci, but also enriched in the perinuclear area where MTOC is localized (Figure 4A, upper panel). Upon colchicine treatment, the microtubule structure was disrupted, and PS-ASO perinuclear accumulation was also abolished (Figure 4A, lower panel). In cells treated with colchicine, PS-ASOs appeared as large clumps scattered in the cytoplasm. As compared with control cells where PS-ASOs showed linear movement over longer distances, disruption of microtubules with colchicine caused Brownian movements of PS-ASO clumps within a short range, as seen from the time projection results (Figure 4B) and a live cell movie (Supplemental Mov-8). These PS-ASO clumps also contained Rab7 (Supplementary Figure S4A), suggesting that LEs clustered upon disruption of microtubules. Similar observations were made when cells were treated with other microtubule disrupting molecules, demecolcine or Nocodazole (Supplementary Figure S4B, C). These results indicate that disruption of the microtubule network abolished perinuclear concentration of PS-ASO containing LEs, leading to LE clumping in the cytoplasm.

To further confirm this observation, HeLa cells incubated with PS-ASO for 6h were fixed, and stained for TUBB, and PS-ASO localization was examined in cells at different stages of the cell cycle. At anaphase/metaphase, cytoplasmic microtubule network disappears, and microtubules attach to sister chromatids and facilitate their separation (32). Therefore, in such cells LE movement along microtubules should be disrupted. Indeed, in a metaphase cell, PS-ASO containing LEs also formed large clumps, and no obvious 'perinuclear' positioning was observed, whereas in the cell at interphase, PS-ASO-LE foci appeared smaller and tended to localize to the perinuclear area where colocalized with the MTOC (Figure 4C). In cells that underwent cytokinesis, in which cytoplasmic microtubule structures were re-established, PS-ASOs again tended to localize to the perinuclear region (Figure 4D). These results together suggest that LE movement along microtubules results in net movement of PS-ASOs to the MTOC region in the perinuclear area where LE movement is slow, causing perinuclear enrichment of PS-ASO containing LEs.

PS-ASO containing LE movement along microtubules can contribute to LE deformation

LE movement along microtubules may contribute to LE fission that may affect PS-ASO release from LEs. To determine if PS-ASO containing LE fission occurs when moving along microtubules, PS-ASO foci movement was recorded in live cells expressing GFP-tubulin. Although in most cases PS-ASO containing foci appeared as round shaped structures, more oblong PS-ASO structures that moved along the microtubule network could also be observed in live cells (Figure 5A, Supplemental mov-9). Such tubular PS-ASO structures contain GFP-Rab7 (Figure 5B), indicative of membraned LEs. We note that tubular LEs are not unique to PS-ASOs, since internalized transferrin could also be observed in tubular LEs in live cells (Supplementary Figure S5), and tubular endosomes have been observed previously (33).

As observed with round shaped PS-ASO-LEs (Supplemental Mov-7), the linear movement of tubular PS-ASO structures also showed a stop-and-go pattern and could change directions when other microtubules were encountered (Supplemental Mov-9). It has been shown that LE movement along microtubules in a cellular environment can be affected by the presence of other structures, such as mitochondria, ER, and actin filaments (34). We also observed that PS-ASO containing LE movement was delayed when an ER structure was encountered, as demonstrated in live cells with GFP-ER labeling (Figure 5C, Supplemental Mov-10). Thus, it is possible that LE movement along microtubules may contribute to the deformation of LE structures and fission/fusion events. Indeed, live cell imaging showed that oblong or tubular PS-ASO-LEs and circular PS-ASO-LEs along microtubules can be linked (Figure 5D), and circular PS-ASO-LEs can stretch out to form tubular shapes (Supplemental Mov-11). The budding of a smaller PS-ASO containing LE from a larger LE can also be mediated by tubular LE structures, as shown in live cells (Figure 5E).

Reduction of dynein 1 disrupted perinuclear positioning of PS-ASO-LEs and reduced PS-ASO activity

Next, we sought to understand how LE movement and positioning may affect PS-ASO activity. Since disruption of global microtubule networks using small molecules may directly or indirectly affect many aspects of cellular processes, making it difficult to interpret, we attempted to determine whether LE perinuclear positioning itself affects PS-ASO activity using more gentle approaches. It has been shown that LE movement along microtubules towards MTOC mainly depends on cytoplasmic Dynein 1, contributing to the perinuclear localization of LEs, whereas Dynein 2 is only required in certain cases especially in limited spaces (28). LE movement toward the plus end of microtubules (peripheral area of cells) is mediated by a group of kinesin proteins (18).

To determine how perinuclear positioning of PS-ASO-LEs affects PS-ASO activity, dynein 1 was reduced by siRNA treatment (Figure 6A). As expected, reduction of Dynein 1, and not Dynein 2 nor Kinesin 5, by siRNA treatment decreased perinuclear positioning of PS-ASO foci,

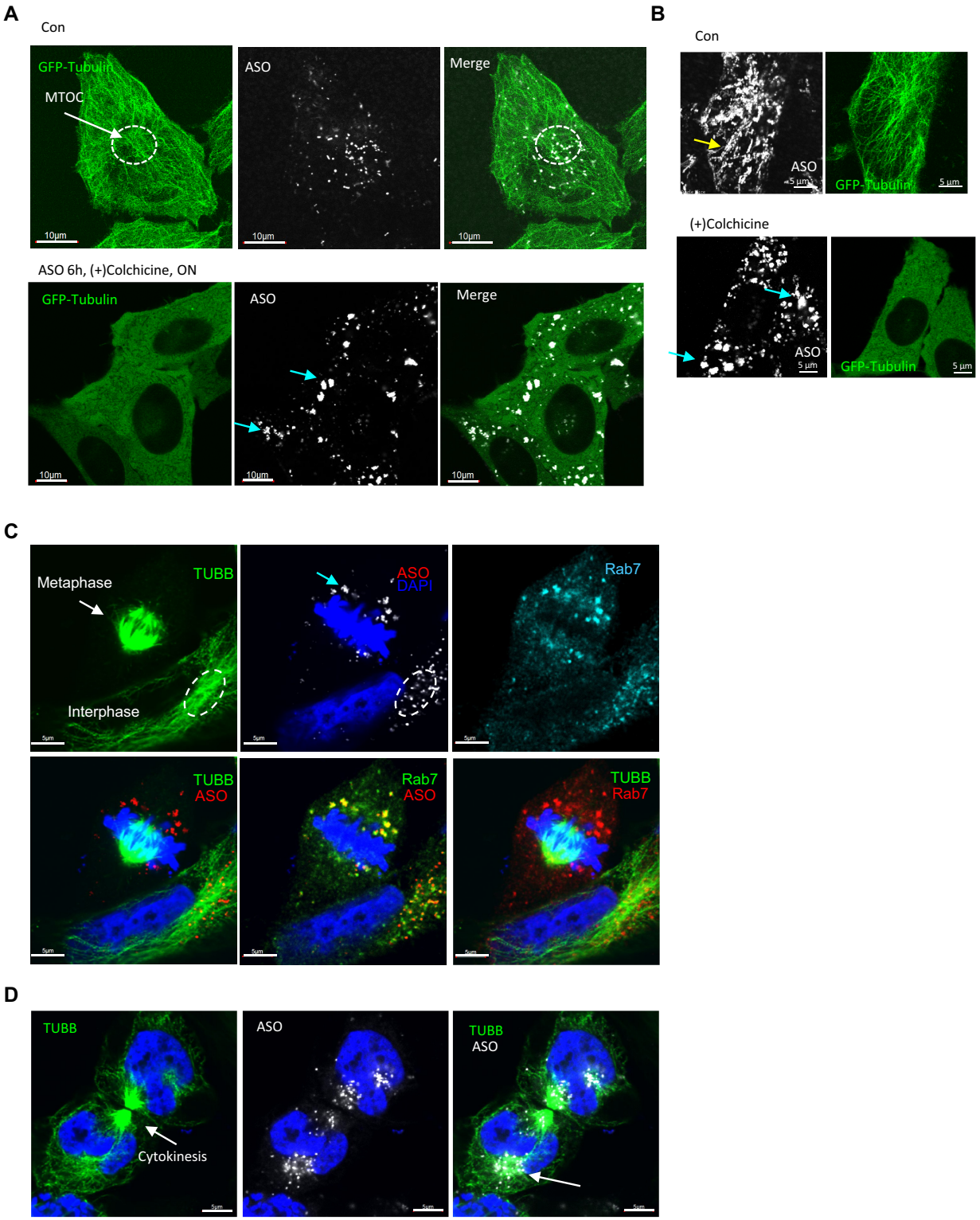

Figure 4. Perinuclear accumulation of PS-ASO-containing LEs depends on microtubule network. (**A**) Live cell imaging of GFP-Tubulin expressing HeLa cells incubated with PS-ASO for 6 h, followed by treatment with either DMSO (upper panels) or 0.15 μg/ml colchicine (lower panels) overnight. The LE aggregation upon colchicine treatment is exemplified in an islet. (**B**) Time projection of PS-ASO foci in cells treated with DMSO (upper panel) or colchicine overnight, as in panel A. Image was recorded for ∼2 min. Linear movement in control cells is marked with a yellow arrow. Brownian movement in colchicine treated cells is exemplified with blue arrows. (**C**) Immunofluorescence staining of TUBB and Rab7 in HeLa cells incubated with 2 μM Cy3-labeled PS-ASO 446654 overnight. MTOC is marked with a dashed circle. A metaphase cell is marked with an arrow. An aggregate of PS-ASO-containing LEs is exemplified with a blue arrow. Scale bars, 5 μm. (**D**) Immunofluorescence staining of TUBB and Rab7 in HeLa cells incubated with 2 μM Cy3-labeled PS-ASO 446654 overnight, as in panel C. A cell in cytokinesis is shown. Perinuclear accumulation of PS-ASO foci is exemplified with an arrow. Nuclei were stained with DAPI.

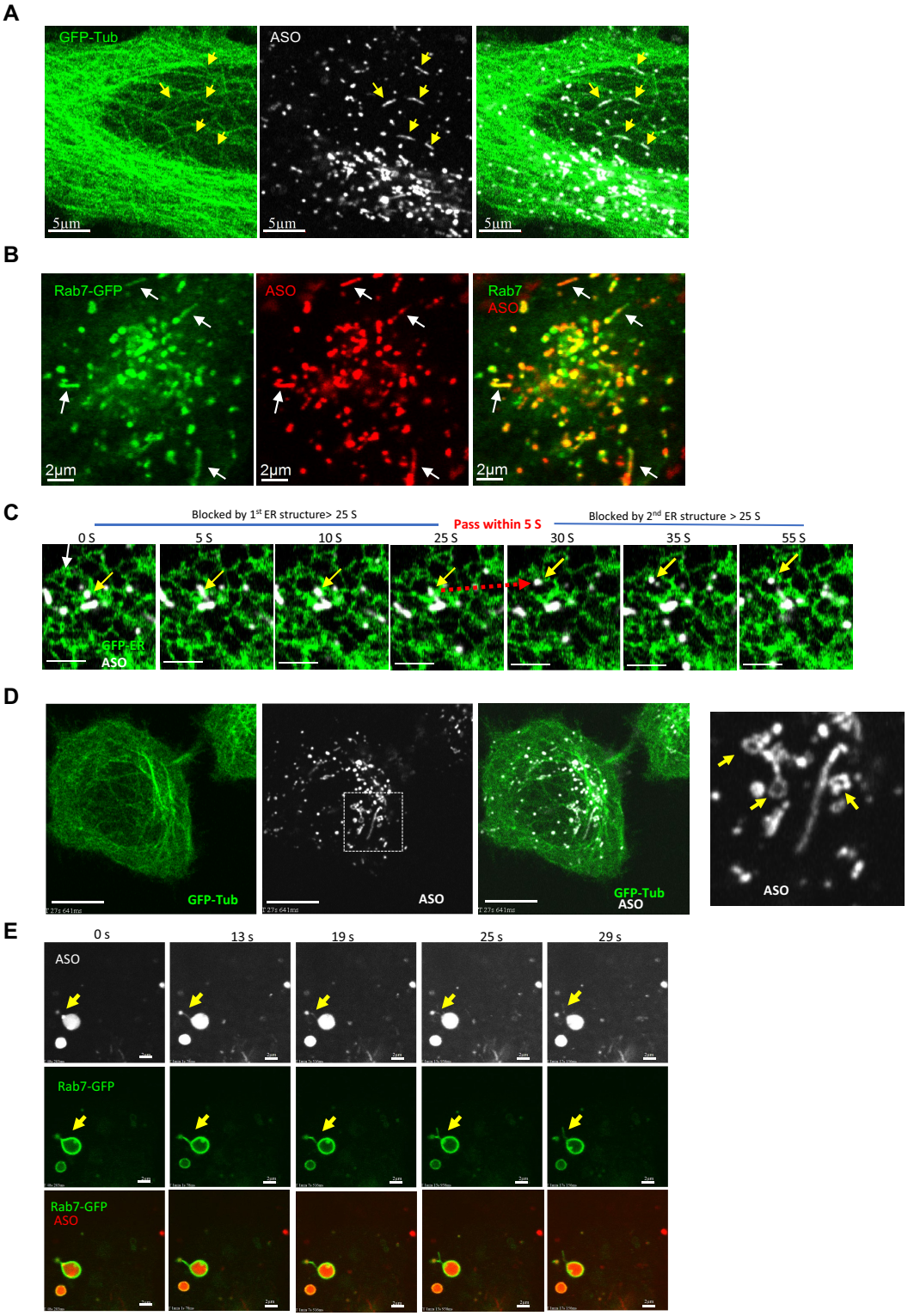

Figure 5. Movement of PS-ASO containing LEs along microtubules can be disrupted by other cellular structures. (**A**) live cell imaging of GFP-Tubulin expressing HeLa cells incubated with PS-ASO for 6 h. The tubular PS-ASO structures along microtubules are marked with yellow arrows. Scale bars, 5 μm. (**B**) Live cell imaging of GFP-LE expressing HeLa cells incubated with PS-ASO for 6 h. The tubular PS-ASO-containing LEs are marked with arrows. Scale bars, 2 μm. (**C**) live cell imaging of GFP-ER expressing HeLa cells incubated with PS-ASO for 6 h. Images were recorded at different times, and snapshots are shown. The movement of a particular PS-ASO foci is marked by arrows. The sudden pass of the blocked PS-ASO focus is marked with a red dashed arrow. Scale bars, 2 μm. (**D**) live cell imaging of GFP-Tubulin expressing HeLa cells incubated with PS-ASO for 6 h. The boxed area is magnified and shown in the right panel. The tubular PS-ASO structures connected with circular PS-ASO structures are marked with arrows. Scale bars, 10 μm. (**E**) Live cell imaging of GFP-LE expressing HeLa cells incubated with PS-ASO for 6 h. Images were recorded at different times and snapshots are shown. The fission of a PS-ASO-containing LE is marked with yellow arrows. Scale bars, 2 μm.

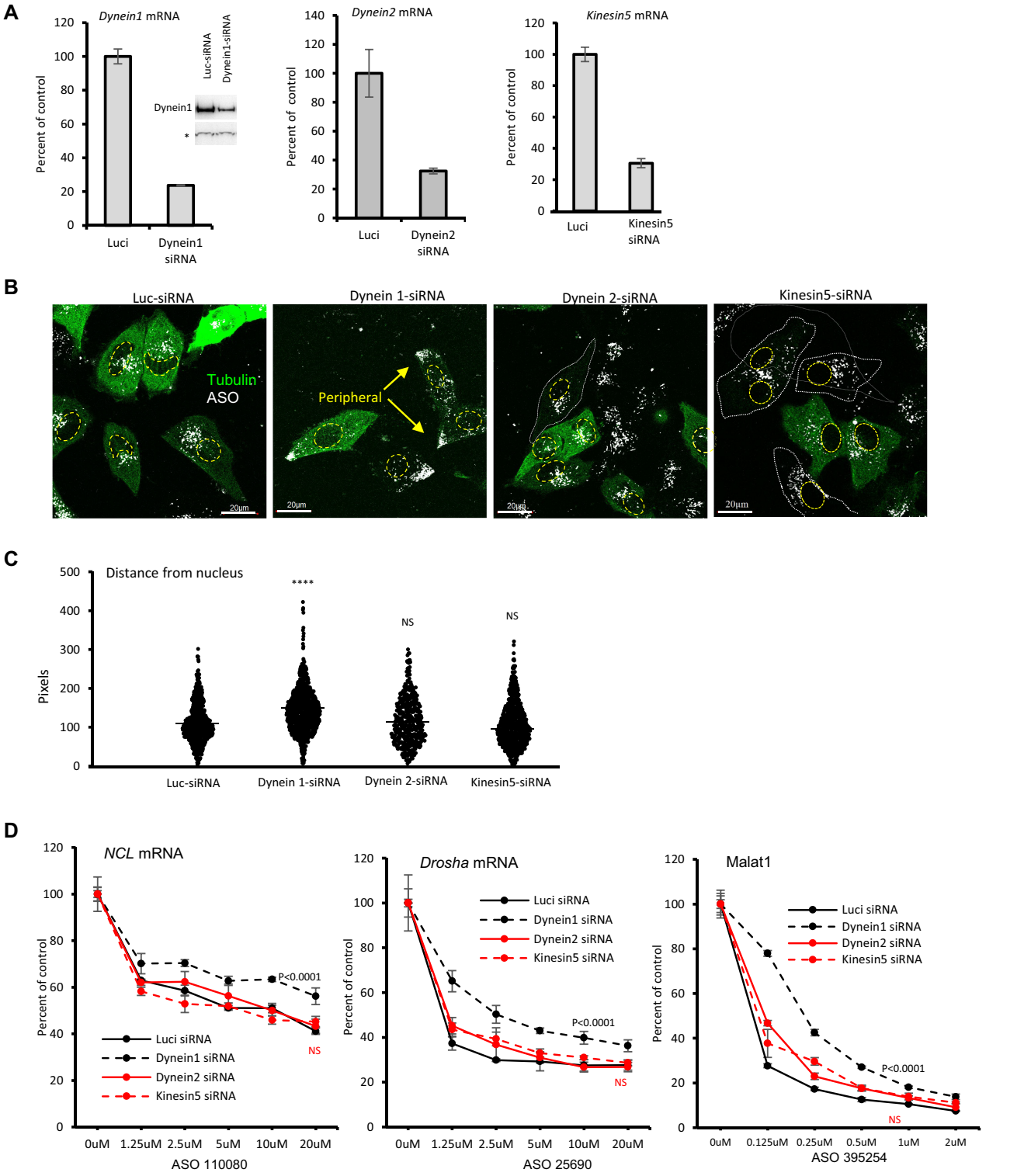

Figure 6. Disruption of perinuclear positioning of PS-ASO foci through modulating Dynein 1 affects PS-ASO activity. (**A**) qRT-PCR quantification of the levels of *Dynein 1*, *Dynein 2*, and *Kinesin 5* mRNAs in HeLa cells transfected with siRNAs for 48 h. Reduction of Dynein 1 protein was also confirmed by western analysis. *, nonspecific band detected with the same antibody that serves as a control for loading. (**B**) Live cell imaging of different siRNA treated HeLa cells that were transduced with virus expressing GFP-tubulin, followed by incubation with 2 μM Cy3-labeled PS-ASO 446654 overnight. Cell shape is marked with white dashed lines, and nucleus with yellow dashed circles. Peripheral accumulation of PS-ASO foci in Dynein 1 reduced cells is marked with arrows. (**C**) Quantification of the distances of PS-ASO foci to the nucleus, as measured from ∼10 cells. P-values were calculated based on unpaired *t*-test using Prism. NS, not significant. ****$P < 0.0001$. (**D**) qRT-PCR quantification of the levels of *NCL*, *drosha,* and Malat1 RNAs in different siRNA treated HeLa cells that were incubated with PS-ASOs overnight. In related panels, error bars are standard deviations from three independent experiments. P values were calculated based on F-test.

leading to more peripheral localization (Figure 6B). The reduced perinuclear positioning can also be seen from the increased distance of ASO foci to the nucleus (Figure 6C). However, reduction of Dynein 1, and not Dynein 2 nor Kinesin 5, decreased PS-ASO activity (Figure 6D). The levels of *NCL*, *drosha* and Malat1 RNAs were not substantially affected by Dynein 1 reduction (Supplementary Figure S6A). Importantly, reduction of Dynein 1 did not affect PS-ASO uptake (Supplementary Figure S6B), and decreased PS-ASO activity was also observed when a different Dynein 1 siRNA was used (Supplementary Figure S6C, D). However, when PS-ASOs were transfected into cells, no activity loss was observed in cells depleted of Dynein 1 (Supplementary Figure S6E, F), suggesting that Dynein 1 may play a role in endosomal release of PS-ASOs upon free uptake.

To further confirm the above effects of Dynein 1 reduction on perinuclear positioning and activity of PS-ASOs, we next evaluated how PS-ASO activity changes upon disruption of perinuclear positioning by over expression of P50 protein, which inhibits dynein functions by disrupting the dynactin complex (35). As expected, overexpression of P50 reduced perinuclear localization of PS-ASO-LEs (Supplementary Figure S7A, B). Importantly, PS-ASO activity was reduced, though modestly, in P50 overexpressed cells (Supplementary Figure S7C), in which PS-ASO uptake was not impaired (Supplementary Figure S6B), similar to the results of Dynein 1 reduction. These observations suggest that LE perinuclear positioning may facilitate PS-ASO activity.

Disruption of perinuclear positioning of PS-ASO-LEs by reduction of RNF26 and its partner proteins also decreased PS-ASO activity

To further confirm the above hypothesis, LE perinuclear positioning was manipulated through different approaches. It has been demonstrated recently that LEs can be tethered to ER at the perinuclear area through interactions with an ER-localized protein RNF26, causing perinuclear positioning of LEs (22). However, RNF26 effects on LE positioning can be reversed by USP15, allowing LE movement along microtubules. Thus, RNF26 was reduced by siRNA treatment (Figure 7A), which led to more scattered localization of PS-ASO foci in the cytoplasm (Figure 7B, C), consistent with previous reports that RNF26 knockdown reduced perinuclear localization of LEs (22). In addition, reduction of RNF26 also decreased the perinuclear positioning of lysosomes, as shown by staining of Lamp1, similar to the situation of Dynein 1 reduction (Supplementary Figure S8A). Importantly, reduction of RNF26 decreased the activities of PS-ASOs upon free uptake (Figure 7D), but not upon transfection (Supplementary Figure S6E, F). PS-ASO-LE linear movement appears not to be substantially affected by RNF26 reduction, as determined in live cells (Supplementary Figure S9). When RNF26 was reduced in mouse hepatocyte derived MHT cells (7), both PS-ASO perinuclear positioning and PS-ASO activity were decreased (Supplementary Figure S10), suggesting that this observation is not unique to certain cell types or species. Although reduction of Dynein 1 caused Golgi fragmentation, reduction of RNF26 did not (Supplementary Figure S8B), consistent with previous reports (22,36). However, reduction of Dynein 1 or RNF26 both decreased perinuclear positioning and activity of PS-ASOs.

It has been demonstrated that tethering of LEs to ER through RNF26 is mediated by other proteins, including SQSTM1 (22). We next reduced this protein by siRNA treatment in HeLa cells (Supplementary Figure S11A). Consistently, reduction of SQSTM1 disrupted perinuclear positioning (Supplementary Figure S11B,C), and reduced PS-ASO activity (Supplementary Figure S11D). Similarly, reduction of SQSTM1 in A431 cells also decreased PS-ASO activity (Supplementary Figure S11E, F). Moreover, reduction of UBE2J1, a protein found most recently to work together with RNF26 in LE tethering to ER (37), decreased the perinuclear positioning and activity of PS-ASOs (Supplementary Figure S12). These results together indicate that perinuclear positioning can enhance PS-ASO activity. This is further supported by the observations that reduction of USP15 enhanced perinuclear aggregation of PS-ASOs (Figure 7E–G). However, reduction of USP15 caused increased activity of PS-ASOs (Figure 7H), as compared with that in control cells. In addition, over-expression of RNF26 also increased perinuclear positioning and activities of PS-ASOs in different cells (Figure 8), further confirming that perinuclear positioning enhances PS-ASO activity. As expected, PS-ASOs also colocalized with Lamp1 (Figure 8), a lysosome marker protein that is also present in some Rab7 positive organelles (38).

DISCUSSION

PS-ASO endosomal trafficking and endosomal release play important roles in ensuring PS-ASO activities. Previously we and others have shown that LEs are the major site for productive release that involves multiple proteins and intracellular vesicles. Here, we characterized PS-ASO movement in the endocytic pathways in the context of cellular structures and found that the movement of LEs along microtubules affect PS-ASO activity, especially the perinuclear positioning, which is required for ensuring PS-ASO activity.

Shortly after internalization, PS-ASOs appear in EEs. EEs move relatively short distances in a Brownian type movement pattern, as determined with live cell imaging. It has been shown that endosomal movement in yeast is mainly along actin filaments, whereas in mammalian cells actin filaments may play a role only in a subset of endocytic budding events (39). Consistently, the movement of PS-ASO containing EEs did not appear to depend on actin filaments in human cells, as evidenced by the observations that PS-ASOs are barely found to move along actin filaments and disruption of actin filaments using latrunculin did not affect PS-ASO activity. This is consistent with previous findings that in mammalian cells actin only affects a subset of clathrin-mediated uptake (18). This observation is also in agreement with the current working model that productive PS-ASO release occurs mainly at LEs (1,3).

Consistent with previous observations that LEs move along microtubules (18), we found that PS-ASOs, mainly present in LEs/lysosomes 40 min after internalization (12), also move along microtubules. This movement is largely linear toward both the peripheral cytoplasmic and the perinuclear areas. Over time, PS-ASO-LEs accumulate in the perinuclear region, where the movement is slower and for

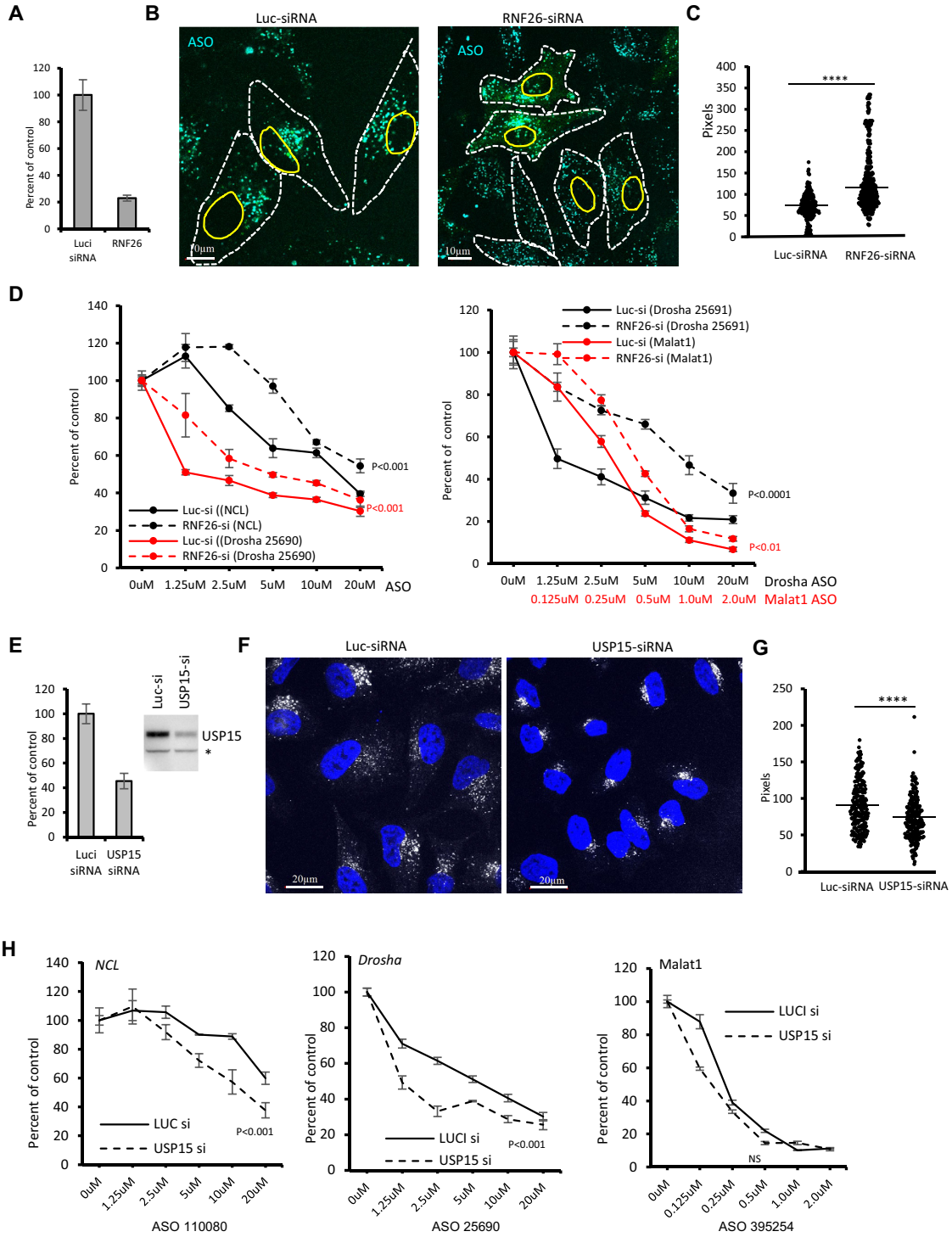

Figure 7. Disruption of perinuclear positioning of PS-ASO foci through modulating ER-LE interaction reduces PS-ASO activity. (**A**) qRT-PCR quantification of the level of *RNF26* mRNA in HeLa cells transfected with siRNAs for 48 h. (**B**) Live cell imaging of siRNA treated HeLa cells incubated with 2 μM Cy3-labeled PS-ASO 446654 overnight. Cell shape and nuclei are marked. Scale bars, 10 μm. (**C**) Quantification of the distances of PS-ASO foci to the nuclei, as measured from ∼10 cells. *P*-values were calculated based on unpaired t-test using Prism. ****$P < 0.0001$. (**D**) qRT-PCR quantification of the levels of *NCL*, *drosha,* and *Malat1* RNAs in different siRNA treated A431 cells that were incubated with PS-ASOs overnight. Error bars are standard deviations from three independent experiments. P values were calculated based on *F*-test using Prism. (**E**) qRT-PCR and western analyses for the levels of *USP15* mRNA and the protein, respectively, in HeLa cells that were treated with siRNAs for 48 h. *, nonspecific band detected with the same antibody that serves as a control for loading. (**F**) Confocal imaging of HeLa cells pre-treated with siRNAs for 48h, followed by incubation of 2 μM Cy3-labeled PS-ASO 446654 overnight. Nuclei were stained with DAPI. (**G**) Quantification of the distances of PS-ASO foci to the nucleus, as measured from ∼10 cells. P-values were calculated based on unpaired *t*-test using Prism. ****, $P < 0.0001$. (**H**) qRT-PCR quantification of the levels of *NCL*, *drosha,* and Malat1 RNAs in different siRNA treated A431 cells that were incubated with PS-ASOs overnight. Error bars are standard deviations from three independent experiments. P values were calculated based on F-test. NS, not significant.

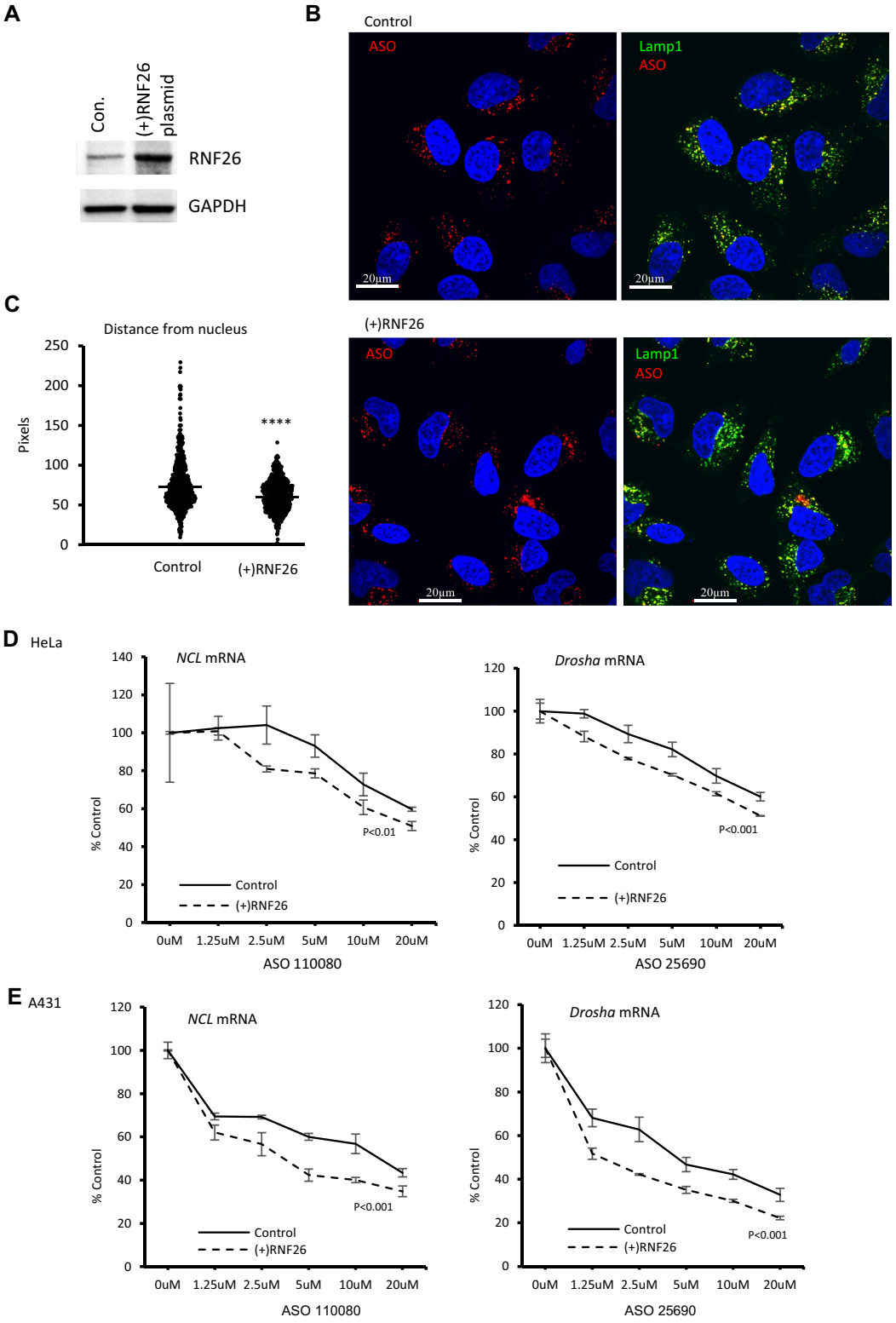

Figure 8. Over-expression of RNF26 enhanced perinuclear accumulation and increased activity of PS-ASOs. (**A**) Western analysis for the levels of RNF26 protein in HeLa cells transfected with an RNF26 expression plasmid for 48 h. GAPDH was detected and served as a control for loading. (**B**) Immunofluorescence staining of Lamp1 in HeLa cells pretreated with siRNAs for 48 h, followed by incubation with 2 μM Cy3-labeled PS-ASO 446654 for 8 h. Scale bars, 20 μm. (**C**) Quantification of the distances of PS-ASO foci to the nuclei, as measured from ∼10 cells. P-values were calculated based on unpaired t-test using Prism. ****$P < 0.0001$. (**D**) qRT-PCR quantification of the levels of *NCL* and *Drosha* mRNAs in control or RNF26 over-expressed HeLa cells that were subsequently incubated with PS-ASOs overnight. (**E**) qRT-PCR quantification of the levels of *NCL* and *Drosha* mRNAs in control or RNF26 over-expressed A431 cells that were subsequently incubated with PS-ASOs overnight. Error bars represent standard deviation from three independent experiments. P values were calculated based on F-test using Prism.

shorter distances compared to that in the peripheral areas of the cytoplasm. The PS-ASO-LE movement occurs in a stop-and-go fashion, as observed previously for endosomes (20). This movement can be affected by other cellular organelles, such as microtubule structures or ER, leading to a pause of PS-ASO-LE movement.

It has been reported that the LEs moving along microtubules may have high membrane tension when they meet other structures (40). Thus, the moving LEs may undergo fission, fusion, and membrane deformation when encountering other organelles. Indeed, we found the PS-ASOs can be present in more tubular LEs along microtubules, which can undergo fission to generate circular LEs. This observation suggests that LE movement along microtubules may affect PS-ASO release during LE fission or membrane deformation. In addition, since many mRNAs are translated on ER membranes, it is possible that PS-ASOs released from LEs associated with the ER may have a higher chance to meet and degrade RNA targets, due to the higher local concentration of PS-ASOs. This possibility is supported by the fact that RNase H1 is also present in the cytosol, in addition to the nucleus and mitochondria, and can act on translating mRNAs (2,41). However, the contribution of PS-ASO release during LE movement to overall PS-ASO activity is unclear, since at early time after PS-ASO internalization (e.g. within 2 h), majority of PS-ASO-LEs are present in periphery areas and move relatively rapidly, however, no PS-ASO activity could be detected at this time (13). At later times (after 6–8 h of PS-ASO internalization) when PS-ASO activity could be detected, PS-ASO-LE foci were found to mainly accumulate in perinuclear areas and moved relatively slowly. It is possible that PS-ASOs released from fast-moving LEs at early time is not sufficient to induce detectable reduction of target RNAs, or that the release of PS-ASOs from fast-moving LEs is weak relative to the release from slow-moving, perinuclear enriched LEs.

The movement of LEs along microtubules contributes to the perinuclear accumulation of PS-ASO-LEs, as microtubule disruption using inhibitors led to PS-ASO-LE clumping in the cytoplasm. Under this condition, the aggregated PS-ASO-LEs move within a short distance in a Brownian fashion. Similar observations were also made in dividing cells in which microtubules disappeared, indicating the importance of microtubules in PS-ASO-LE positioning, consistent with previous reports (18). Perinuclear positioning of LEs appears to be important for PS-ASO activity. Disruption of perinuclear positioning of PS-ASO-LEs through siRNA-mediated reduction of Dynein 1 or over expression of P50 all reduced PS-ASO activity, suggesting that perinuclear positioning may enhance PS-ASO release. This possibility is supported by the following observations: (i) reduction of RNF26, an ER-localized protein responsible for tethering of LEs to ER, reduced PS-ASO activity and perinuclear positioning; (ii) reduction of SQSTM1, a protein required for RNF26 function in perinuclear positioning of LEs, also decreased perinuclear positioning and PS-ASO activity; (iii) depletion of UBE2J1, a protein that works together with RNF26 to mediate LE tethering to ER, similarly reduced perinuclear positioning and activity of PS-ASOs. On the other hand, when perinuclear positioning of PS-ASO foci was enhanced by reduction of USP15 or by over-expression of RNF26, PS-ASO activity was increased. These results indicate that perinuclear positioning of PS-ASO-LEs can enhance PS-ASO activity, most likely by facilitating PS-ASO release, since PS-ASO uptake was not substantially affected. The importance of perinuclear positioning in PS-ASO activity is also supported by a previous observation that more perinuclear accumulation of PS-ASOs was found in cell types showing better PS-ASO activity (42).

PS-ASOs that colocalized with Lamp1 can be found in the perinuclear areas (Figure 8), raising a possibility that PS-ASOs can also be released from lysosomes. Though such a possibility cannot be completely excluded, previous data from our and other's studies suggest that LEs are the major sites for PS-ASO release (9,43). In addition, since many Lamp1 positive organelles are also Rab7 positive (38), it is possible that many such Lamp1 stained organelles may not be bona fide lysosomes. Interestingly, since Golgi are also present in the perinuclear areas, and ER-Golgi transport mediated by COPII vesicles as well as TGN-LE transport pathway mediated by M6PR are known to play important roles in PS-ASO release (5,11,13,44), the perinuclear positioning of PS-ASO-LEs may thus provide an ideal spatial arrangement that facilitates PS-ASO release through Golgi-derived vesicles.

Together, in this study we characterized the PS-ASO endosomal movement in live cells, and showed that LE movement along microtubules plays important roles in ensuring PS-ASO activity, especially perinuclear positioning that tends to enhance PS-ASO release. These observations, together with our previous identifications of multiple proteins and intracellular trafficking pathways that affect PS-ASO productive release, will pave the way towards the development of approaches that enhance PS-ASO release and improve PS-ASO drug potency.

DATA AVAILABILITY

Research data is available upon request. No data was deposited to databases.

SUPPLEMENTARY DATA

Supplementary Data are available at NAR Online.

ACKNOWLEDGEMENTS

We wish to thank Cheryl Li De Hoyos for technique assistance, and Frank Bennett for stimulating discussions.

FUNDING

Internal funding from Ionis Pharmaceuticals. Funding for open access charge: Internal funding from Ionis Pharmaceuticals.

Conflict of interest statement. All authors are employees and shareholders of Ionis Pharmaceuticals.

REFERENCES

1. Crooke,S.T., Wang,S., Vickers,T.A., Shen,W. and Liang,X.H. (2017) Cellular uptake and trafficking of antisense oligonucleotides. *Nat. Biotechnol.*, **35**, 230–237.

2. Liang,X.H., Sun,H., Nichols,J.G. and Crooke,S.T. (2017) RNase H1-dependent antisense oligonucleotides are robustly active in directing RNA cleavage in both the cytoplasm and the nucleus. *Mol. Ther.*, **25**, 2075–2092.
3. Juliano,R.L. (2018) Intracellular trafficking and endosomal release of oligonucleotides: what we know and what we don't. *Nucleic Acid Ther.*, **28**, 166–177.
4. Miller,C.M., Donner,A.J., Blank,E.E., Egger,A.W., Kellar,B.M., Ostergaard,M.E., Seth,P.P. and Harris,E.N. (2016) Stabilin-1 and Stabilin-2 are specific receptors for the cellular internalization of phosphorothioate-modified antisense oligonucleotides (ASOs) in the liver. *Nucleic Acids Res.*, **44**, 2782–2794.
5. Liang,X.H., Sun,H., Nichols,J.G., Allen,N., Wang,S., Vickers,T.A., Shen,W., Hsu,C.W. and Crooke,S.T. (2018) COPII vesicles can affect the activity of antisense oligonucleotides by facilitating the release of oligonucleotides from endocytic pathways. *Nucleic Acids Res.*, **46**, 10225–10245.
6. Buntz,A., Killian,T., Schmid,D., Seul,H., Brinkmann,U., Ravn,J., Lindholm,M., Knoetgen,H., Haucke,V. and Mundigl,O. (2019) Quantitative fluorescence imaging determines the absolute number of locked nucleic acid oligonucleotides needed for suppression of target gene expression. *Nucleic Acids Res.*, **47**, 953–969.
7. Koller,E., Vincent,T.M., Chappell,A., De,S., Manoharan,M. and Bennett,C.F. (2011) Mechanisms of single-stranded phosphorothioate modified antisense oligonucleotide accumulation in hepatocytes. *Nucleic Acids Res.*, **39**, 4795–4807.
8. Juliano,R.L. (2016) The delivery of therapeutic oligonucleotides. *Nucleic Acids Res.*, **44**, 6518–6548.
9. Wang,S., Sun,H., Tanowitz,M., Liang,X.H. and Crooke,S.T. (2017) Intra-endosomal trafficking mediated by lysobisphosphatidic acid contributes to intracellular release of phosphorothioate-modified antisense oligonucleotides. *Nucleic Acids Res.*, **45**, 5309–5322.
10. Crooke,S.T., Vickers,T.A. and Liang,X.H. (2020) Phosphorothioate modified oligonucleotide-protein interactions. *Nucleic Acids Res.*, **48**, 5235–5253.
11. Liang,X.H., Sun,H., Hsu,C.W., Nichols,J.G., Vickers,T.A., De Hoyos,C.L. and Crooke,S.T. (2020) Golgi-endosome transport mediated by M6PR facilitates release of antisense oligonucleotides from endosomes. *Nucleic Acids Res.*, **48**, 1372–1391.
12. Wang,S., Sun,H., Tanowitz,M., Liang,X.H. and Crooke,S.T. (2016) Annexin A2 facilitates endocytic trafficking of antisense oligonucleotides. *Nucleic Acids Res.*, **44**, 7314–7330.
13. Liang,X.H., Nichols,J.G., De Hoyos,C.L., Sun,H., Zhang,L. and Crooke,S.T. (2021) Golgi-58K can re-localize to late endosomes upon cellular uptake of PS-ASOs and facilitates endosomal release of ASOs. *Nucleic Acids Res.*, **49**, 8277–8293
14. Bonifacino,J.S. and Neefjes,J. (2017) Moving and positioning the endolysosomal system. *Curr. Opin. Cell Biol.*, **47**, 1–8.
15. Akhmanova,A. and Steinmetz,M.O. (2015) Control of microtubule organization and dynamics: two ends in the limelight. *Nat. Rev. Mol. Cell Biol.*, **16**, 711–726.
16. Bild,A.H., Turkson,J. and Jove,R. (2002) Cytoplasmic transport of Stat3 by receptor-mediated endocytosis. *EMBO J.*, **21**, 3255–3263.
17. Cabukusta,B. and Neefjes,J. (2018) Mechanisms of lysosomal positioning and movement. *Traffic*, **19**, 761–769.
18. Granger,E., McNee,G., Allan,V. and Woodman,P. (2014) The role of the cytoskeleton and molecular motors in endosomal dynamics. *Semin. Cell Dev. Biol.*, **31**, 20–29.
19. Reck-Peterson,S.L., Redwine,W.B., Vale,R.D. and Carter,A.P. (2018) The cytoplasmic dynein transport machinery and its many cargoes. *Nat. Rev. Mol. Cell Biol.*, **19**, 382–398.
20. Neefjes,J., Jongsma,M.M.L. and Berlin,I. (2017) Stop or go? Endosome positioning in the establishment of compartment architecture, dynamics, and function. *Trends Cell Biol.*, **27**, 580–594.
21. Raiborg,C., Wenzel,E.M. and Stenmark,H. (2015) ER-endosome contact sites: molecular compositions and functions. *EMBO J.*, **34**, 1848–1858.
22. Jongsma,M.L., Berlin,I., Wijdeven,R.H., Janssen,L., Janssen,G.M., Garstka,M.A., Janssen,H., Mensink,M., van Veelen,P.A., Spaapen,R.M. *et al.* (2016) An ER-associated pathway defines endosomal architecture for controlled cargo transport. *Cell*, **166**, 152–166.
23. Liang,X.H., Vickers,T.A., Guo,S. and Crooke,S.T. (2011) Efficient and specific knockdown of small non-coding RNAs in mammalian cells and in mice. *Nucleic Acids Res.*, **39**, e13.
24. Liang,X.H., Shen,W., Sun,H., Prakash,T.P. and Crooke,S.T. (2014) TCP1 complex proteins interact with phosphorothioate oligonucleotides and can co-localize in oligonucleotide-induced nuclear bodies in mammalian cells. *Nucleic Acids Res.*, **42**, 7819–7832.
25. Schindelin,J., Arganda-Carreras,I., Frise,E., Kaynig,V., Longair,M., Pietzsch,T., Preibisch,S., Rueden,C., Saalfeld,S., Schmid,B. *et al.* (2012) Fiji: an open-source platform for biological-image analysis. *Nat. Methods*, **9**, 676–682.
26. Girao,H., Geli,M.I. and Idrissi,F.Z. (2008) Actin in the endocytic pathway: from yeast to mammals. *FEBS Lett.*, **582**, 2112–2119.
27. Matteoni,R. and Kreis,T.E. (1987) Translocation and clustering of endosomes and lysosomes depends on microtubules. *J. Cell Biol.*, **105**, 1253–1265.
28. Reck-Peterson,S.L., Redwine,W.B., Vale,R.D. and Carter,A.P. (2018) The cytoplasmic dynein transport machinery and its many cargoes. *Nat. Rev. Mol. Cell Biol.*, **19**, 382–398.
29. Joshi,H.C. (1993) Gamma-tubulin: the hub of cellular microtubule assemblies. *BioEssays*, **15**, 637–643.
30. Zhu,X. and Kaverina,I. (2013) Golgi as an MTOC: making microtubules for its own good. *Histochem. Cell Biol.*, **140**, 361–367.
31. Nolasco,S., Bellido,J., Serna,M., Carmona,B., Soares,H. and Zabala,J.C. (2021) Colchicine blocks tubulin heterodimer recycling by tubulin cofactors TBCA, TBCB, and TBCE. *Front. Cell Dev. Biol.*, **9**. 656273.
32. Carlton,J.G., Jones,H. and Eggert,U.S. (2020) Membrane and organelle dynamics during cell division. *Nat. Rev. Mol. Cell Biol.*, **21**, 151–166.
33. Villaseñor,R., Schilling,M., Sundaresan,J., Lutz,Y. and Collin,L. (2017) Sorting tubules regulate blood-brain barrier transcytosis. *Cell Rep.*, **21**, 3256–3270.
34. Wijdeven,R.H., Jongsma,M.L., Neefjes,J. and Berlin,I. (2015) ER contact sites direct late endosome transport. *BioEssays*, **37**, 1298–1302.
35. Burkhardt,J.K., Echeverri,C.J., Nilsson,T. and Vallee,R.B. (1997) Overexpression of the dynamitin (p50) subunit of the dynactin complex disrupts dynein-dependent maintenance of membrane organelle distribution. *J. Cell Biol.*, **139**, 469–484.
36. Palmer,K.J., Hughes,H. and Stephens,D.J. (2009) Specificity of cytoplasmic dynein subunits in discrete membrane-trafficking steps. *Mol. Biol. Cell*, **20**, 2885–2899.
37. Cremer,T., Jongsma,M.L.M., Trulsson,F., Vertegaal,A.C.O., Neefjes,J. and Berlin,I. (2021) The ER-embedded UBE2J1/RNF26 ubiquitylation complex exerts spatiotemporal control over the endolysosomal pathway. *Cell Rep.*, **34**, 108659.
38. Humphries,W.H.t., Szymanski,C.J. and Payne,C.K. (2011) Endo-lysosomal vesicles positive for Rab7 and LAMP1 are terminal vesicles for the transport of dextran. *PLoS One*, **6**, e26626.
39. Girao,H., Geli,M.-I. and Idrissi,F.-Z. (2008) Actin in the endocytic pathway: From yeast to mammals. *FEBS Lett.*, **582**, 2112–2119.
40. Zajac,A.L., Goldman,Y.E., Holzbaur,E.L. and Ostap,E.M. (2013) Local cytoskeletal and organelle interactions impact molecular-motor- driven early endosomal trafficking. *Curr. Biol.*, **23**, 1173–1180.
41. Liang,X.H., Nichols,J.G., Sun,H. and Crooke,S.T. (2018) Translation can affect the antisense activity of RNase H1-dependent oligonucleotides targeting mRNAs. *Nucleic Acids Res.*, **46**, 293–313.
42. Linnane,E., Davey,P., Zhang,P., Puri,S., Edbrooke,M., Chiarparin,E., Revenko,A.S., Macleod,A.R., Norman,J.C. and Ross,S.J. (2019) Differential uptake, kinetics and mechanisms of intracellular trafficking of next-generation antisense oligonucleotides across human cancer cell lines. *Nucleic Acids Res.*, **47**, 4375–4392.
43. Yang,B., Ming,X., Cao,C., Laing,B., Yuan,A., Porter,M.A., Hull-Ryde,E.A., Maddry,J., Suto,M., Janzen,W.P. *et al.* (2015) High-throughput screening identifies small molecules that enhance the pharmacological effects of oligonucleotides. *Nucleic Acids Res.*, **43**, 1987–1996.
44. Liang,X.H., Nichols,J.G., Hsu,C.W. and Crooke,S.T. (2021) Hsc70 facilitates mannose-6-phosphate receptor-mediated intracellular trafficking and enhances endosomal release of phosphorothioate-modified antisense oligonucleotides. *Nucleic Acid Ther.*, **31**, 284–297